Carbohydrate Polymers 76 (2009) 607–615

Contents lists available at ScienceDirect

Carbohydrate Polymers

journal homepage: www.elsevier.com/locate/carbpol

Bionanocomposites based on pea starch and cellulose nanowhiskers hydrolyzed from pea hull fibre: Effect of hydrolysis time

Yun Chen [a,b], Changhua Liu [c], Peter R. Chang [a,*], Xiaodong Cao [a], Debbie P. Anderson [a]

[a] Bioproducts and Bioprocesses National Science Program, Agriculture and Agri-Food Canada, 107 Science Place, Saskatoon, SK, Canada S7N 0X2
[b] Research Centre for Medical and Structural Biology, School of Basic Medical Science, Wuhan University, Wuhan 430071, China
[c] College of Chemistry and Chemical Engineering, Southwest University, Chongqing 400715, China

ARTICLE INFO

Article history:
Received 18 October 2008
Received in revised form 13 November 2008
Accepted 18 November 2008
Available online 6 December 2008

Keywords:
Bionanocomposite
Nanowhisker
Reinforcement
Hydrolysis time
Starch
Pea hull fibre

ABSTRACT

By hydrolyzing pea hull fibres (PHF) for different times (*t*) with sulfuric acid, a series of pea hull fibre-derived nanowhisker (PHFNW-*t*) dispersions was prepared. The PHFNW-*t* dispersions were then blended with pea starch (PS) to fabricate bionanocomposite films (PS/PHFNW-*t*). The effect of *t* on the structure and properties of the PHFNW-*t* nanowhiskers and those of the corresponding PS/PHFNW-*t* nanocomposite films were investigated. The length (*L*), diameter (*D*) and *L*/*D* values of the PHFNW-*t* ranged from 240 to 400 nm, 7 to 12 nm, and 32.22 to 36.00, respectively. The PS/PHFNW-*t* nanocomposite films exhibited higher ultraviolet absorption, transparency, tensile strength, elongation at break, and water-resistance than both the neat PS film and the PS/PHF film (as a control with a *t* of 0 h). The PS/PHFNW-8 film showed the highest transparency, tensile strength, and elongation at break among the PS/PHFNW-*t* films, due to the high *L*/*D* of PHFNW-8. These results revealed that the length of hydrolysis time had a great effect on the structure (including *L*, *D* and *L*/*D*) of the PHFNW-*t* nanowhiskers, as well as on the structure and performance of the resulting PS/PHFNW-*t* films. For preparation of PHFNW-*t* nanowhiskers and corresponding PS/PHFNW-*t* films, the most suitable hydrolysis time, in this work, is 8 h.

1. Introduction

Since their announcements about using cellulose whiskers in 1995 (Favier, Chanzy, & Cavaillé, 1995; Favier et al., 1995; Gauthier & Perez, 1995), the application of cellulose nanowhiskers as reinforcement in nanocomposites has attracted significant attention (Azizi Samir, Alloin, & Dufresne, 2005; Chazeau, Cavaillé, Canova, Dendievel, & Boutherin,1999; Choi & Simonsen, 2006; Helbert, Cavaillé, & Dufresne, 1996; Wang, Sain, & Oksman, 2007). This interest is due to cellulose's renewable nature, abundance and good mechanical properties, and to the large specific surface area of the nanowhiskers. The interfacial area and the theoretical elastic modulus have been reported to be more than 100 m^2/g (Favier et al., 1995) and 167.5 GPa (Tashiro & Kobayashi, 1991), respectively. The homogeneous distribution of the nanowhiskers within the matrix and the strong interactions and adhesions with the polymer matrix, have resulted in obvious improvements in the mechanical properties of nanocomposites. The structure and properties, especially the size of the nanowhiskers, depend on the source of the original cellulose materials (Araki, Wada, Kuga, & Okano, 1998; Kvien, Tanem, & Oksman, 2005; Revol, Bradford, Giasson, Marchessault, & Gray, 1992) and on the preparation process (Ye, 2007). Several methods for preparing nanowhiskers have been developed in recent years (Cheng, Wang, Rials, & Lee, 2007; Ye, 2007). These methods include physical treatments, e.g. shearing or high-pressure homogenizing (Pääkkö et al., 2007; Takagi & Asano, 2007); chemical treatments, e.g. acid hydrolysis (Bondeson, Mathew, & Oksman, 2006); biological treatments, e.g. enzyme-assisted hydrolysis (Hayashi, Kondo, & Ishihara, 2005; Henriksson, Henriksson, Berglund, & Lindström, 2007); synthetic and electrospinning methods (Frenot, Henriksson, & Walkenström, 2007), as well as a combinations of the methods mentioned above (Pääkkö et al., 2007).

Among the methods developed to extract nanowhiskers from cellulose, acid hydrolysis is the most well-known and widely used (Bondeson et al., 2006). Nickerson and Habrle (1947) disclosed the use of hydrochloric and sulfuric acid hydrolysis to produce crystallites from cellulose materials, and Ranby reported the preparation of cellulose whiskers from microfibrils, also using acid hydrolysis (Ranby, 1952). Marchessault and co-workers studied the hydrolysis of chitin and native, mercerized and bacterial cellulose to prepare nanocrystals/nanowhiskers with birefringence (Marchessault, Morehead, & Koch, 1961; Marchessault, Morehead, & Walter, 1959). Beck-Candanedo, Roman, and Gray (2005) have investigated the effects of reaction time and acid/pulp ratio on the properties of nanocrystals and suspensions when hydrolyzing black spruce acid sulfite pulp. Dong, Revol, and Gray (1998) have

* Corresponding author. Tel.: +1 306 956 7637; fax: +1 306 956 7247.
E-mail address: Changp@agr.gc.ca (P.R. Chang).

0144-8617/$ - see front matter Crown Copyright © 2008 Published by Elsevier Ltd. All rights reserved.
doi:10.1016/j.carbpol.2008.11.030

prepared colloidal suspensions of cellulose microcrystals from filter paper by sulfuric acid hydrolysis. The particle properties and the phase separation of the suspensions were strongly dependent on the hydrolysis temperature and time, and on the intensity of the ultrasonic irradiation used to disperse the particles. Bondeson et al. (2006) recommended optimized processing conditions using the sulfuric acid hydrolysis method to separate individual crystallites/whiskers from microcrystalline cellulose (MCC). With a sulfuric acid concentration of 63.5% (w/w), it was possible to produce cellulose whiskers, with a length of between 200 and 400 nm and a width of less than 10 nm, in approximately 2 h with a yield of 30% (Bondeson et al., 2006). These optimized parameters in the hydrolysis process would have been different if the cellulose had come from different sources or had been pre-treated in different ways before hydrolysis. However, reports on the relationships between the hydrolysis conditions of the nanowhiskers and the performance of the nanocomposites were scarce.

We have successfully obtained pea hull fibre-derived nanowhiskers (PHFNW) by sulfuric acid hydrolysis of pea hull fibre (PHF) and used the PHFNW as filler to prepare nanocomposite films with pea starch (PS) in our lab (Chen, Liu, Anderson, Huneault, & Chang, 2009). PHFNW extracted from PHF by acid-hydrolysis for 4 h showed a significant reinforcement when the filler content was 5–10 wt% in the PS-based composite films. Based on that work, we further hypothesized that nanowhiskers hydrolyzed from PHF under different conditions would have different effects on the properties of the PS-based composite films when they were used as filler in a pea starch matrix. If conditions such as acid concentration, acid/fibre ratio, and hydrolysis temperature are consistent, hydrolysis time will then play a key role in the properties of the resulting nanowhiskers. In this work, we prepared a series of nanowhiskers with different hydrolysis times and then used them as filler in fabricating pea starch-based bionanocomposite films. The effects of hydrolysis time on the structure and properties of the nanowhiskers, as well as on the corresponding pea starch-based bionanocomposite films, were investigated.

2. Experimental method

2.1. Materials

Pea hull fibre (PHF, Centara III™, prepared from the hulls of Canadian Yellow Peas) and pea starch (Accu-Gel™, prepared from Canadian Yellow Peas), both food grade, were supplied by Nutri-Pea Limited Canada (Portage la Prairie, Canada). Pea hull fibre and pea starch were vacuum-dried at 50 °C for 24 h before use. Sulfuric acid (95.7%) was purchased from Fisher Scientific (Fair Lawn, NJ, USA). Glycerol (99.5%) and other chemicals were from Sigma–Aldrich Inc. (St. Louis, MO, USA) and used without further purification.

2.2. Preparation of pea hull fibre-derived nanowhisker dispersion

The pea hull fibre-derived nanowhisker (PHFNW) dispersion in water was prepared by the acid hydrolysis process (Bondeson et al., 2006; Dong, Kimura, Revol, & Gray, 1996.). Briefly, pea hull fibre (PHF, 30 g) was mixed with sulfuric acid solution (250 mL, 64 wt%) and stirred vigorously at 45 °C. After a period of time, the mixture was partially neutralized with sodium hydroxide aqueous solution (40 wt%), and decoloured by sodium hypochlorite solution. The mixture was washed by successive centrifugations with deionized water until neutrality was achieved. It was dialysed for 3 days and then diluted with deionized water to give a PHFNW dispersion with a nanowhisker concentration of around 2 wt%. The dispersion did not sediment or flocculate because of the surface sulfate groups that were created during the sulfuric acid treatment (Dong et al., 1998). By changing the hydrolysis time i.e. 4, 8, 12, 16 and 24 h, a series of PHFNW dispersions was prepared and coded as PHFNW-*t*, where *t* was the hydrolysis time. For example, PHFNW-8 means the nanowhiskers were hydrolyzed from PHF by sulfuric acid for 8 h.

Table 1
Codes for nanowhiskers hydrolyzed from PHF by sulfuric acid with different hydrolysis times (*t*), and their length (*L*), diameter (*D*) and average axial ratio of length and diameter (*L*/*D*) measured by AFM.

Sample code	*t* (h)	Size (average ± *SD*)		
		L (nm)	*D* (nm)	*L*/*D*
PHF	0	34,000 ± 21,000	14,000 ± 6000	2.43
PHFNW-4	4	400 ± 130	12 ± 6	33.33
PHFNW-8	8	360 ± 120	10 ± 3	36.00
PHFNW-12	12	290 ± 80	9 ± 3	32.22
PHFNW-16	16	270 ± 80	8 ± 3	33.75
PHFNW-24	24	240 ± 50	7 ± 3	34.29

2.3. Preparation of PS/PHFNW-t, PS/PHF and PS films

Fabrication of PS/PHFNW-*t*, PS/PHF and PS films was based on a solution casting and evaporation process (Lu, Weng, & Cao, 2006). Pea starch and PHFNW-*t* (*t* = 4, 8, 12, 16 or 24 h) was fixed at a weight ratio of 90:10. Glycerol content based on pea starch and PHFNW-*t* was fixed at 30 wt%. PS, glycerol, and PHFor PHFNW-*t* were mixed in deionized water and heated at 100 °C for 30 min with stirring until the mixture gelatinized. The mixture was then degassed, cast in a polystyrene Petri dish and dried at 40 °C overnight to obtain composite films with a thickness of approximately 0.16 mm. The film was coded as PS/PHFNW-*t*. For instance, PS/PHFNW-4 means the film was prepared with PS as the matrix and PHFNW-4 as filler. A control film was prepared by blending PS and PHF (which was not hydrolyzed by acid, i.e. the hydrolysis time *t* = 0) according to the same process using PHF instead of PHFNW-*t*. At the same time, a neat PS film without PHFNW-*t* or PHF added was obtained via the process mentioned above. The codes and compositions of the films are listed in Table 1. The films were kept at room temperature in a conditioning desiccator at 43% relative humidity (RH was conditioned by K_2CO_3 saturated solution) for 7 days before tests.

2.4. Characterizations

2.4.1. Morphology of the PHF and PHFNW-t

The morphology of PHF was observed by a scanning electron microscope (SEM, S-4800, Hitachi, Ibaraki, Japan). The dried PHF particles were coated with gold and then observed with an accelerating voltage of 10 kV by SEM. The morphology of the PHFNW-*t* powders was observed by an atomic force microscope (AFM). PHFNW-*t* samples were prepared by dropping 30 μL of aqueous PHFNW-*t* solution (0.001 wt%) onto poly-L-lysine coated mica, incubating for 1–2 min, rinsing with Millipore water, and gently drying with nitrogen. Samples were stored in covered Petri dishes until measurements were done (generally within 12 h of sample preparation). Atomic force microscope measurements were carried out on a PicoSPM instrument (Molecular Imaging, Tempe, AZ, USA) with a scanner operating in acoustic intermittent contact mode. A TESPA silicon cantilever (Veeco, Santa Barbara, CA, USA) was used for imaging. All measurements were performed at ambient conditions with the instrument mounted in a vibration isolation system. The scan rate was 0.5–1 lines/s (512 pixels per line) for all images. The length (*L*), diameter (*D*, measured from the height of the nanowhiskers) and the *L*/*D* values of the nanowhiskers were obtained from the AFM images using PicoScan V5.3 software (Molecular Imaging, Tempe, AZ, USA).

2.4.2. FTIR analysis of the PHF and PHFNW-t powders, and the films

Attenuated Total Reflectance Fourier Transform Infrared (ATR-FTIR) spectra of the film samples were recorded on a Nicolet

5700 FTIR spectrometer (Thermo Electron Corporation, Waltham, MA, USA). The dried film samples were taken at random from the flat films and data was collected at room temperature over 16 scans with a resolution of 4 cm^{-1}. The PHF or the vacuum-dried PHFNW-*t* powders were mixed with KBr to laminate for the FTIR analysis at a wavenumber range of 4000–400 cm^{-1}.

2.4.3. XRD analysis of the PHF and PHFNW-t powders, and the films

Wide-angle X-ray diffraction patterns of the PHF and PHFNW-*t* powders, and the films were recorded on a Bruker AXS X-ray diffraction instrument (Bruker AXS Inc., Madison, WI, USA), using CuK_α radiation (λ = 0.154 nm) at 40 kV and 30 mA with a scan rate of 4° min^{-1}. The diffraction angle (2θ) ranged from 4° to 40°.

2.4.4. Morphology of the films

A scanning electron microscope (SEM, S-570, Hitachi, Ibaraki, Japan) was used to observe the morphology of the PS, PS/PHF and PS/PHFNW-*t* composite films. The films were frozen in liquid nitrogen and snapped immediately, and then the cross-sections of the films were coated with gold and observed with an accelerating voltage of 20 kV.

2.4.5. Light transmittance testing of the films

The light transmittance (T_r) of the PS, PS/PHF and PS/PHFNW-*t* films with a thickness of 0.16 mm was measured using an ultraviolet–visible (UV–Vis) spectroscope (UV-160A, Shimadzu, Japan) at a wavelength range of 200–800 nm.

2.4.6. Thermogravimetric and differential thermogravimetry analysis of the films

Thermogravimetric (TG) analysis and differential thermogravimetry (DTG) of the films were carried out on a TA-STDQ600 (TA Instruments Inc., New Castle, DE, USA). The thermograms were acquired between 30 and 480 °C at a heating rate of 10 °C/min. Nitrogen was used as the purge gas at a flow rate of 20 mL/min. An empty pan was used as a reference.

2.4.7. Tensile testing of the films

The tensile strength (σ_b) and elongation at break (ε_b) of the films were measured on a universal testing machine (CMT 6503, Shenzhen SANS Test Machine Co. Ltd., Shenzhen, China) at room temperature with gauge length of 5 cm and crosshead speed of 50 mm/min. The average value of four replicates for each sample was taken.

2.4.8. Moisture uptake of the films

The moisture uptake of PS, PS/PHF and PS/PHFNW-*t* films was determined. The samples used were thin rectangular strips with dimension of 50 × 10 × 0.1 mm. They were vacuum-dried at 60 °C overnight and then kept at 0% RH (P_2O_5) for one week. After weighing, they were conditioned at room temperature in a desiccator at 98% RH ($CuSO_4{\cdot}5H_2O$ saturated solution) for one week. The moisture uptake (M_u) of the samples was calculated as follows:

$$M_u = (W_1 - W_0)/W_0 \times 100\%$$

where W_0 and W_1 were the weight of the sample before exposure to 98% RH and after one week, respectively. The average value of three replicates for each sample was used.

3. Results and discussion

3.1. Morphology of the PHF and PHFNW

An SEM photograph of PHF and AFM photographs of PHFNW are shown in Fig. 1. The measured average length (*L*), diameter (*D*) and *L*/*D* of the PHF and PHFNW-*t* are listed in Table 1. The original PHF exhibited an irregular shape and size (about 34 ± 21 μm in length and 14 ± 6 μm in width, estimated from Fig. 1A); however, the PHFNW-*t* hydrolyzed from PHF by sulfuric acid was needle-like or rod-like nanowhiskers (Fig. 1B–F). The average *L* and *D* of the PHFNW-*t* nanowhiskers was much smaller than that of the PHF, and showed a dependence on the hydrolysis time (*t*). With an increase in *t* from 4 to 24 h, the *L* ranged from 400 to 240 nm, and *D* from 12 to 7 nm. The *L*/*D* values of the PHFNW-*t* nanowhiskers were much higher than that of PHF, while the *L*/*D* values of PHFNW-*t* changed slightly (not more than 11%) with an increase in *t*. Interestingly, the PHFNW-8 (*t* = 8 h) showed the highest *L*/*D* value (36.00), which may play an important role in the physical properties of the nanowhiskers and the corresponding PS/PHFNW-8 film, as described later.

3.2. FTIR analysis of the PHF and PHFNW-t powders, and the films

The FTIR spectra of the original PHF and extracted PHFNW-*t* are illustrated in Fig. 2A. The FTIR spectra of the PHF and PHFNW-*t* are very consistent with those of soy hulls and acid-treated soy hulls, respectively, as reported by Alemdar and Sain (2008). The peaks at 3413 and 1635 cm^{-1} in the spectra of both PHF and PHFNW-*t* are attributed to the stretching and bending vibrations, respectively, of the hydrogen bonding –OH groups of cellulose (Sain & Panthapulakkal, 2006). The peaks at 1058 and 896 cm^{-1} are related to the C–O stretching and C–H rocking vibrations of cellulose (Alemdar & Sain, 2008). Compared with the FTIR spectra of PHF, a few changes can be observed in that of PHFNW-*t* as a result of the chemical treatment. For example, the peak at 1735 cm^{-1}, attributed to either the acetyl and uronic ester groups of the hemicelluloses or to the ester linkage of the carboxylic groups of ferulic and *p*-coumeric acids in lignin and/or hemicelluloses, occurred in the spectra of PHF (Sun, Xu, Sun, Fowler, & Baird, 2005). However, this peak disappeared completely in the spectra of PHFNW-*t* due to the removal of most of the hemicelluloses and lignin from the PHF during the acid extraction process. The peak at 1245 cm^{-1} in the spectra of PHF is associated with the C–H, O–H or CH_2– bending frequencies. This peak also almost disappeared in PHFNW-*t*, further indicating the removal of the corresponding groups linked with lignin in PHF. The differences in the FTIR spectrum between PHF and PHFNW-*t* indicate that PHFNW-*t*, with high cellulose content, has been successfully extracted from PHF by sulfuric acid hydrolysis treatment. No obvious changes were observed in the FTIR of the PHFNW-*t* with different *t* values, indicating that the chemical groups in the resulting PHFNW-*t* were stable, and that no strong chemical reactions occurred when *t* increased from 4 to 24 h. The chemical removal of the hemicelluloses and lignin from the PHF was mostly complete in the first 4 h of acid hydrolysis.

The FTIR spectra of the PS, PS/PHF and PS/PHFNW-*t* films are illustrated in Fig. 2B. The peaks at 3282, 1652 and 999 cm^{-1} in the spectra of PS were attributed, respectively, to stretching vibrations of the hydrogen bonding –OH groups, bending vibrations of –OH groups and stretching vibrations of C–O in starch (Chen, Cao, Chang, & Huneault, 2008; Zhang & Han, 2006). Due to the chemical similarities between starch and cellulose, and to the relatively low content (10 wt%) of nanowhiskers within the PS matrix, the PS/PHFNW-*t* composite films exhibited almost the same FTIR spectra as the PS film. The characteristic absorption of cellulose at around 896 cm^{-1} in PHFNW-*t* was also not obvious in the PS/PHFNW-*t* composites. The –OH bending and C–O stretching vibrations in PS were located at 3283 and 1652 cm^{-1}, respectively. They shifted to 3278–3284 and 1633–1646 cm^{-1}, respectively, in the spectra of the PS/PHFNW-*t* films, suggesting that new hydrogen bonding interactions between cellulose and starch molecules formed as a result of the addition of cellulose nanocrystals into starch. Only very slight shifts in absorption relating to –OH bending and C–O

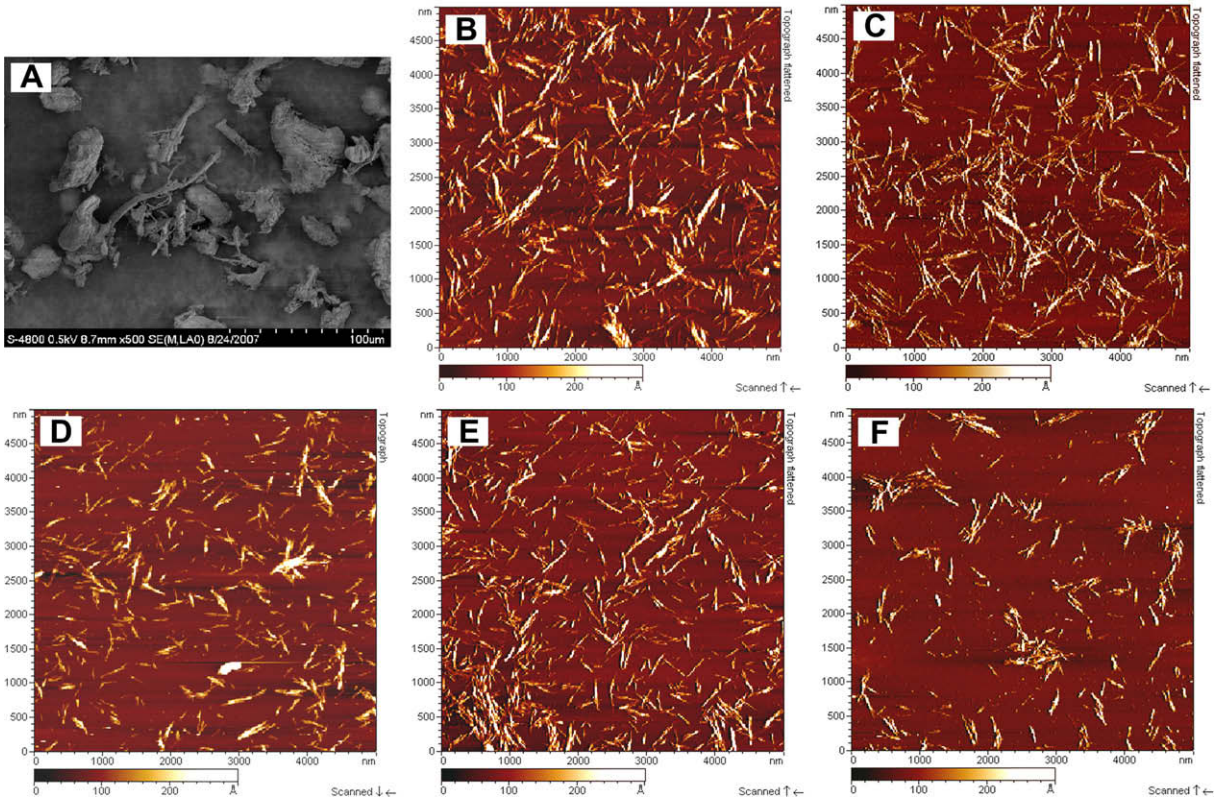

Fig. 1. SEM photograph of PHF (A) and AFM photographs of PHFNW-4 (B), PHFNW-8 (C), PHFNW-12 (D), PHFNW-16 (E) and PHFNW-24 (F). Scales are shown on photographs.

stretching vibrations took place in the PS/PHFNW-*t* films with different *t*.

3.3. XRD analysis of the PHF and PHFNW-t powders, and the films

The XRD patterns of the PHF and PHFNW-*t* are shown in Fig. 3A. Both PHF and PHFNW-*t* showed obvious diffraction peaks, at 22.2° to 22.5° respectively, attributed to the cellulose component (Wang et al., 2007). The PHF exhibited peaks at about $2\theta = 22.2°$, 30.7° and 34.7°, and a broad hump around 15.3° showing the amorphous nature. PHFNW-*t* showed a highly crystalline feature with a strong narrow peak at $2\theta = 22.5°$ and relatively lower peaks at $2\theta = 14.9°$, 16.3° and 34.6°. This is a XRD pattern typical of cellulose-I-type crystalline structure, which is very similar to the cotton linters reported in our previous work (Luo et al., 2008). This indicated that the chemical composition of PHFNW-*t* was high purity in terms of cellulose. The peak at around 22° is sharper in the PHFNW-*t* than in the PHF. Though no data for the degree of crystallinity was provided, the sharper diffraction peak is an indication of a higher degree of crystallinity in the structure of the PHFNW (Wang et al., 2007). This is due to the partial removal of the amorphous regions during the acid-hydrolysis treatment of PHF (Alemdar & Sain, 2008).

With an increase in *t*, the XRD patterns of the PHFNW-*t* changed slightly. The peaks at around 22.5° and 15° of the PHFNW-8, PHFNW-12 and PHFNW-16 seem sharper than those of the PHFNW-4 and PHFNW-24. With an increase in hydrolysis time from 4 to 8 h, the relative intensity of the peak at around 22.5° increased. When the hydrolysis time was greater than 8 h, there was no obvious increase in the relative intensity of this diffraction peak. This indicated that 8 h of hydrolysis was long enough to remove most of the amorphous regions in PHF. With further hydrolysis, particularly as hydrolysis time reached 24 h, the cellulose crystalline regions in the nanowhiskers were partially destroyed due to corrosion from the concentrated sulfuric acid. This kind of damage in the cellulose crystalline regions may decrease the flexibility of the nanowhiskers.

The XRD of the nanocomposite films is shown in Fig. 3B. For the PS film, a typical C-type crystallinity pattern with peaks at $2\theta = 5.6°$ (characteristic of B type polymorphs), 17.1° (characteristic of both A and B type polymorphs), 20.1° and 22.5° (characteristic of B type polymorphs) were clearly observed (Ratnayake, Hoover, & Warkentin, 2002). With the addition of PHFNW-*t* to the starch matrix, the peaks at $2\theta = 14.7°$, 16.4°, and 22.7°, which correspond to the XRD pattern of cellulose I, are observed. This shows that the cellulose nanowhiskers still retain their crystallinity within the PS matrix. Due to the low percentage of nanowhiskers (10 wt%) in the matrix and to the destruction of starch crystallinity during the gelation process, the addition of cellulose nanowhiskers to PS did not obviously change the locations and intensities of the starch peaks in XRD. As a result, all the PS/PHFNW-*t* nanocomposite films appeared to have XRD patterns that were very similar to the PS film.

3.4. Morphology of the films

The SEM photographs of the cross-sections of PS, PS/PHF and PS/PHFNW-*t* films are shown in Fig. 4. It was observed that the cross-sections of the neat PS film (A) were smooth, while the PS/PHF composite film (B) was very rough. This was due to the micro-scale fillers and obvious aggregates of PHF within the PS matrix. The cross-sections of the PS/PHFNW-*t* nanocomposites (C–F) were also rougher than the PS film, due to the incorporation of PHFNW-*t* as filler; however, they seemed much smoother than the corresponding PS/PHF film, indicating that PHFNW-*t*, with a higher aspect ratio and smaller size, formed a stronger interaction with PS than

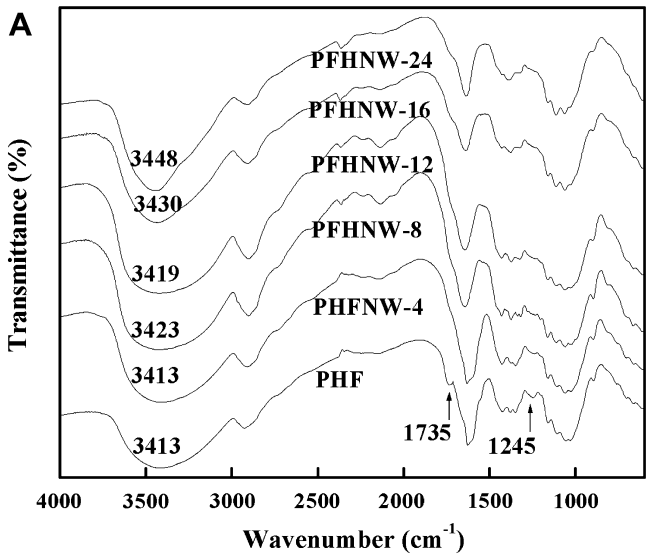

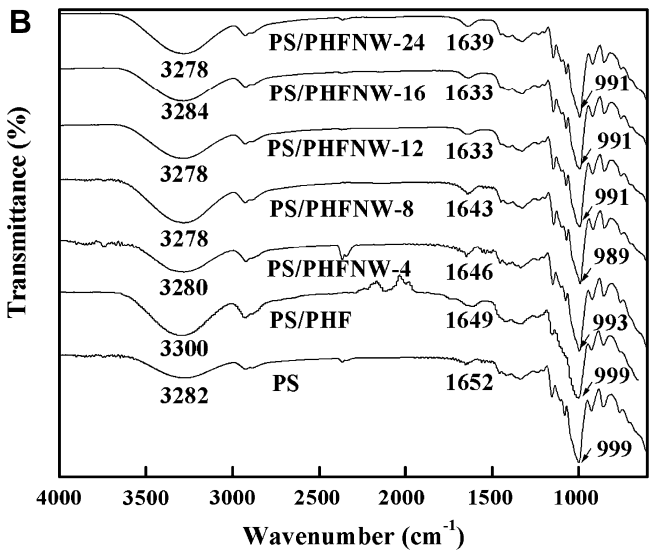

Fig. 2. FTIR spectra of PHF and freeze–dried PHFNW-*t* powders, and PS, PS/PHF, and PS/PHFNW-*t* (*t* = 4, 8, 12, 16, and 24 h) films.

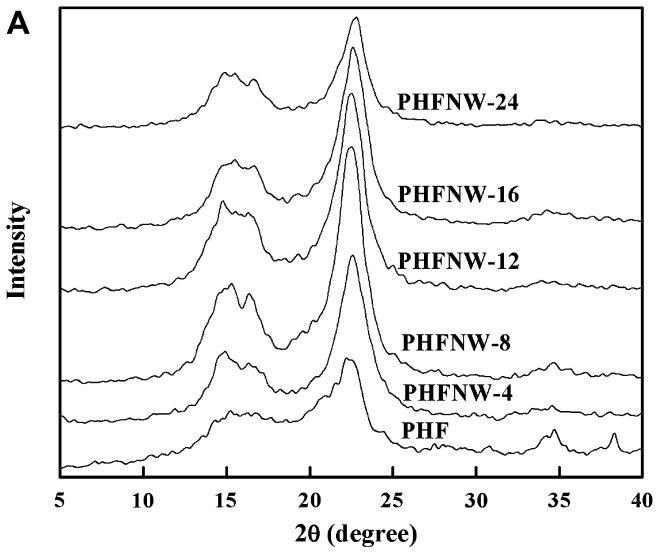

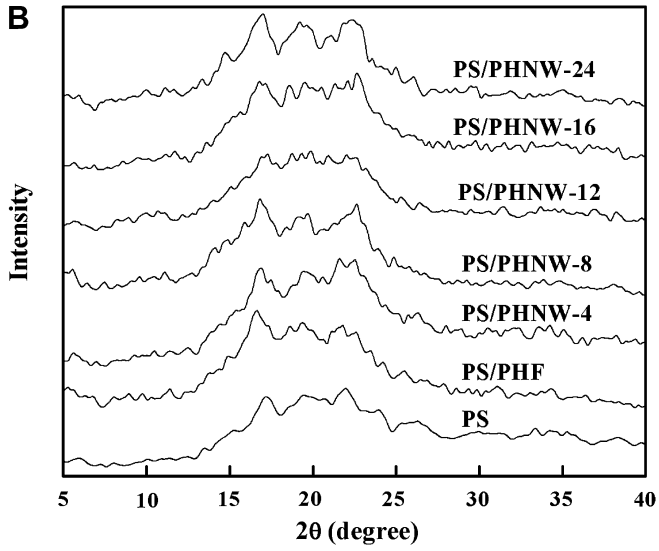

Fig. 3. XRD patterns of PHF and freeze–dried PHFNW-*t* powders, and PS, PS/PHF, and PS/PHFNW-*t* (*t* = 4, 8, 12, 16, and 24 h) films.

PHF could, and dispersed more homogenously than PHF within PS matrix.

The effects of *t* on the micro-structure of the corresponding films could be identified by the differences in the morphology of the fracture surfaces of the composite films. The particle-like nanowhiskers could be found on the cross-sections of the PS/PHFNW-*t* films, showing a successful fabrication of nanocomposite films. On the cross-sections of the PS/PHFNW-4 (C), PS/PHFNW-8 (D) and PS/PHFNW-12 (E) films, the nanowhiskers look like they were wrapped or covered by the PS matrix. Some of the nanowhiskers on the cross-sections of the PS/PHFNW-24 film (F) however, stood out and looked naked after fracturing. This difference shows that the PHFNW-4, PHFNW-8 and PHFNW-12 nanowhiskers had stronger interactions and adhesion with the PS matrix than the PHFNW-24 did. Particularly, the cross-section of the PS/PHFNW-8 was smoother than that of the other nanocomposite films, showing a more homogeneous dispersion of PHFNW-8 within PS. Fewer outstanding particle-like nanowhiskers were observed on the cross-section of the PS/PHFNW-8, suggesting PHFNW-8 was wrapped more tightly by the PS matrix. This stronger adhesion between PHFNW-8 and PS will contribute to the improvement in the toughness of the PS/PHFNW-8 composite film, as shown later.

3.5. Light transmittance testing of the films

The light transmittance (T_r) of the selected films in the wavelength range of 200–800 nm is shown in Fig. 5. The T_r value of PS/PHF film was significantly lower than that of the neat PS film at the same wavelength, indicating that the filling of PHF in PS decreased the transparency of the films. For example, at a wavelength of 800 nm, the T_r values of PS/PHF and PS were 39.4% and 56.8%, respectively. This was due to the microscale size of PHF and, especially, to the heterogeneous dispersion of PHF within the PS matrix, as revealed by SEM. On the whole, the T_r values of PS/PHFNW-*t* films were much lower than those of neat PS at wavelengths from 200 to 400 nm, indicating that the addition of PHFNW-*t* to PS increased the absorption of ultraviolet light of the composite films. It is interesting to note that the absorption of ultraviolet light for the composite films obviously increased as the hydrolysis time of the corresponding PHFNW-*t* increased. Furthermore, the T_r values of PS/PHFNW-*t* films were very close to, and even higher than,

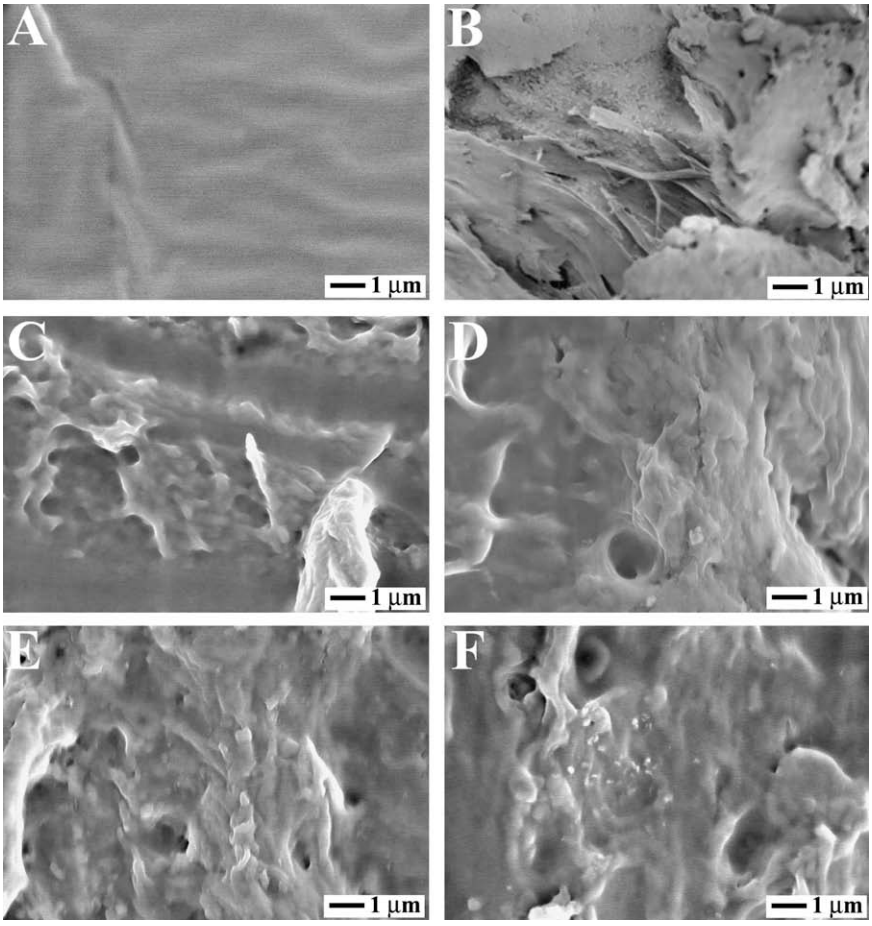

Fig. 4. SEM photographs of the cross-sections of PS (A), PS/PHF (B) and PS/PHFNW-*t* (C: PS/PHFNW-4; D: PS/PHFNW-8; E: PS/PHFNW-12; F: PS/PHFNW-24) films.

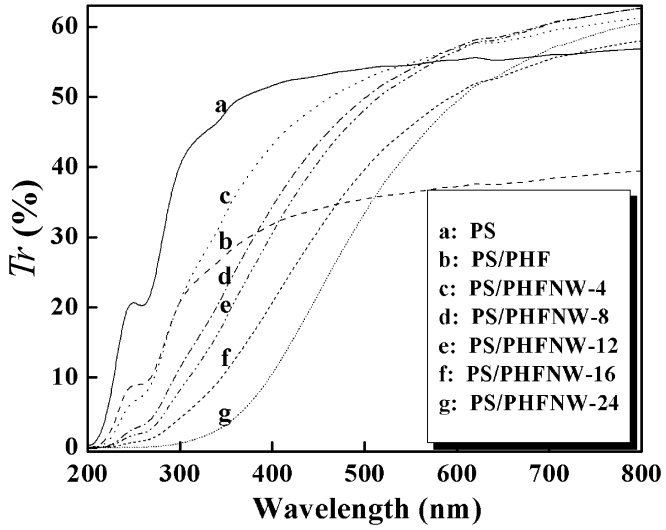

Fig. 5. Light transmittance (T_r) of PS, PS/PHF and PS/PHFNW-*t* (*t* = 4, 8, 12, 16, and 24 h) films over wavelength range of 200–800 nm.

those of the neat PS film at wavelengths from 600 to 800 nm, indicating that the addition of PHFNW-*t* into PS did not decrease the transparency of the composite films and even, to a certain degree, enhanced the transparency of the composite films. This was attributed to the nanometer size effects of PHFNW-*t*, resulting from the homogeneous dispersion of nanoscaled PHFNW-*t* within PS and to strong interactions between the nanowhiskers and matrix. In the wavelength range of 600–800 nm, the PS/PHFNW-8 showed the highest T_r values of all the films, indicating the highest transparency. The results from the transmittance measurement of the films at wavelengths from 200 to 800 nm showed that the addition of PHFNW-*t* into PS improved the performance of anti-ultraviolet radiation while keeping or enhancing the transparency of the resulting nanocomposite films.

3.6. Thermogravimetric and differential thermogravimetry analysis

Thermogravimetric (TG) analysis and differential thermogravimetry (DTG) curves of the films are shown in Fig. 6A and B, respectively. The corresponding data are listed in Table 2. The TG and DTG curves reveal the weight loss of the material as it is heated. The gradual weight loss of the samples was due to the evaporation of water and glycerol and to the dehydration and decomposition of the polymers (Mathew & Dufresne, 2002). The T_{max} value corresponds to the temperature at a maximum rate of mass loss. As shown in Table 2, the T_{max} of PS and PS/PHF were 311.5 and 324.5°C, showing that the PS/PHF film had a higher thermal stability than PS; however, the T_{max} of PS/PHFNW-*t* decreased from 310.7 to 298.7°C with an increase in *t* from 4 to 24 h. This suggested that the thermal stability of the PS/PHFNW-*t* composite films decreased with an increase in *t*. As reported by Roman and Winter (2004), the presence of acid sulfate groups would decrease the thermal stability of cellulose because of the dehydration reaction. As a result, the thermal decomposition temperature of cellulose nanowhiskers prepared by sulfuric acid-treatment was lower

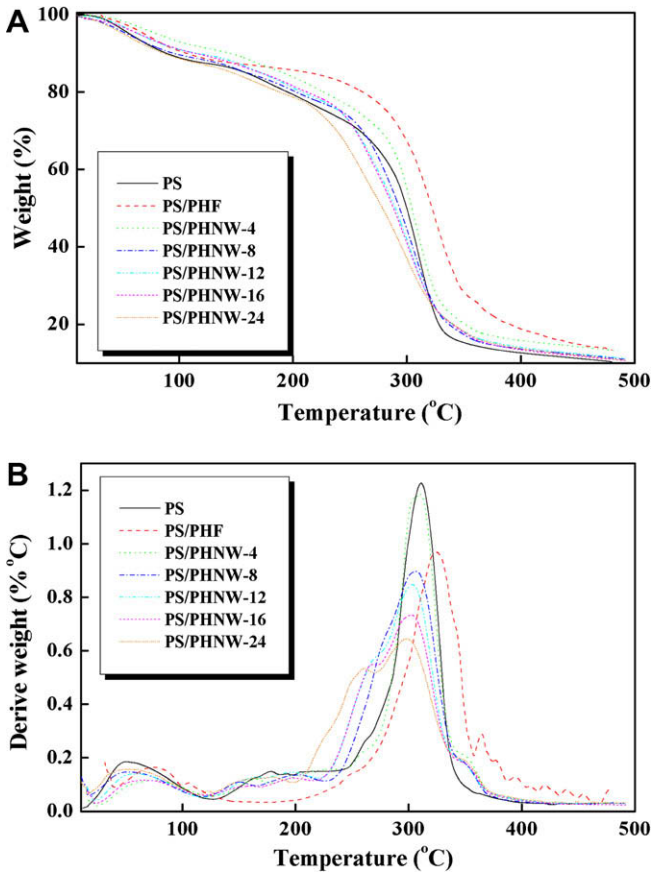

Fig. 6. TGA and DTG curves of PS, PS/PHF and PS/PHFNW-*t* (*t* = 4, 8, 12, 16, and 24 h) films.

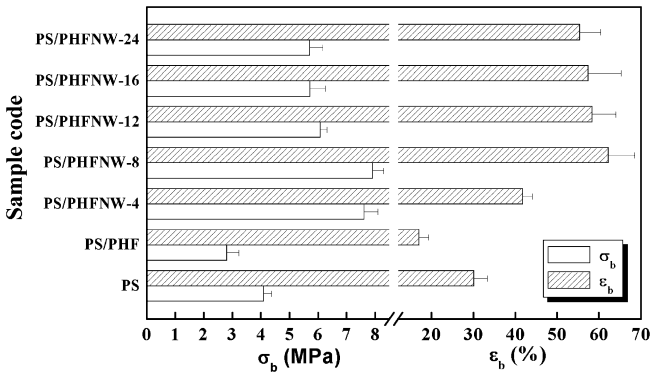

Fig. 7. Tensile strength (σ_b) and elongation at break (ε_b) of PS and PS/PHFNW-*t* (*t* = 4, 8, 12, 16, and 24 h) films.

than that of the original cellulose (Wang, Ding, & Cheng, 2007). The thermal stability of PHFNW-*t* decreased as the hydrolysis time increased due to the longer interaction time between PHF and sulfuric acid during the hydrolysis period. Thus, the thermal stability of the composite films PS/PHFNW-*t* decreased as *t* increased.

3.7. Mechanical properties of the films

Fig. 7 shows the tensile strength (σ_b) and elongation at break (ε_b) of PS, PS/PHF and PS/PHFNW-*t* films. The σ_b and ε_b values of the neat PS film were 4.1 MPa and 30.1%, respectively. The σ_b and ε_b values of the PS/PHF composite film (2.8 MPa and 17.0%, respectively) were lower than those of the neat PS film. This indicated that due to the heterogeneous size distribution and agglomerations of PHF within the PS matrix, PHF did not act as reinforcing filler in PS. However, on the whole PS/PHFNW-*t* films exhibited higher σ_b and ε_b values than both the neat PS film and the PS/PHF-*t* films. As stated, the results of morphology observation and optical property tests show that PHFNW-*t* were nanoscale in size, had a large aspect ratio and homogeneous dispersion within PS. The strong interactions between PHFNW-*t* and PS molecules which formed during the film-making process lead to an obvious enhancement in the mechanical properties of the resulting nanocomposite films. This showed that PHFNW-*t*, as a nanoscale filler, played a significant role in the reinforcement of the matrix. It was worth noting that the σ_b and ε_b values of PS/PHFNW-8 (σ_b = 7.9 MPa, and ε_b = 62.2%) were the highest, which were respectively, 1.9- and 2.0-fold those of the neat PS film, and 2.8- and 3.6-fold those of the PS/PHF film. With an increase in *t* from 8 to 24 h, both the σ_b and ε_b values of PS/PHFNW-*t* films decreased slightly, but were still higher than those of the neat PS film. The PS/PHFNW-8, PS/PHFNW-12, PS/PHFNW-16 and PS/PHFNW-24 films showed much higher ε_b values than that of PS/PHFNW-4, indicating that a *t* of not less than 8 h is necessary for improved toughness of the resulting composite films. Thus, the hydrolysis time had a greater effect on the toughness than on the tensile strength of the composite films.

3.8. Moisture uptake of the films

Moisture uptake (M_u) of the films under 98% RH for 7 days is shown in Fig. 8. The M_u of PS in this condition was 74.1%, which was higher than for other films containing PHF or PHFNW-*t*. This indicated that the addition of PHF-based fillers, either in micro- or nanoscale size, decreased the moisture uptake of the PS-based composites. The content of the PS, fillers and glycerol was consistent in all the composite films, thus the difference in the M_u of the films may be attributed to the degree of water-sensitivity of

Table 2
Code and composition of the PS-based films and the T_{max} from the results of TG and DTG analysis.

Sample code	Filler within the matrix	Compositions in the films		T_{max} (°C)
		Filler content (wt%)[a]	Glycerol content (wt%)[b]	
PS	–	0	30	311.5
PS/PHF	PHF	10	30	324.5
PS/PHFNW-4	PHFNW-4	10	30	310.7
PS/PHFNW-8	PHFNW-8	10	30	306.5
PS/PHFNW-12	PHFNW-12	10	30	303.5
PS/PHFNW-16	PHFNW-16	10	30	301.8
PS/PHFNW-24	PHFNW-24	10	30	298.7

[a] Fillers content = Fillers/(starch + fillers).
[b] Glycerol content = Glycerol/(starch + fillers + glycerol).

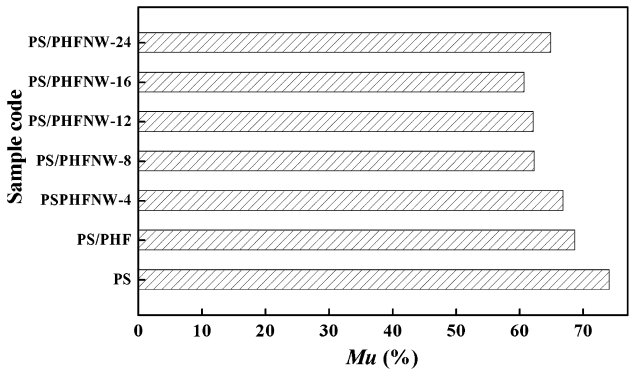

Fig. 8. Moisture uptake (M_u) of PS, PS/PHF-*n* and PS/PHFNW-*t* (*t* = 4, 8, 12, 16, and 24 h) films at RH of 98% for 7 days.

the fillers within PS. The M_u of PS/PHF, 68.6%, was higher than that of the PS/PHFNW-*t* films (M_u = 66.8%, 62.3%, 62.2%, 60.7% and 64.9%, when *t* = 4, 8, 12, 16 and 24 h, respectively), meaning that the nanowhiskers had higher water-resistance than the original PHF. The factors affecting the water-resistance of the fillers with the same chemical composition are the relative content of the crystalline regions and the aspect ratios. With an increase in PHF hydrolysis time, the cellulose crystalline regions in the nanowhiskers increased, resulting in an increase in water-resistance; when the aspects of the nanowhiskers increased, water-resistance decreased. As a result, the M_u of the PS/PHFNW-*t* decreased slightly as *t* increased from 4 to 16 h. When *t* was 24 h, the M_u of PS/PHFNW-24 increased again. This may be attributed to the partial destruction of the cellulose crystalline regions in PHFNW-24 because of long hydrolysis period, as shown in XRD results.

3.9. The relationship among the hydrolysis time of PHFNW-t, the structure of PHFNW-t and the properties of the resulting PS/PHFNW-t composite films

In this work, the hydrolysis time (*t*) of the PHFNW-*t* played an important role in the structure of PHFNW-*t* (the size including *L* and *D*, as well as the *L*/*D*) and the properties (optical, thermal, mechanical properties and water-resistance) of the PS/PHFNW-*t* composite films.

Both the *L* and *D* of PHF are microscale in size, while the *L* and *D* of PHFNW-*t* are nanoscale sized due to acid hydrolysis. As a result, the PS/PHFNW-*t* composite films exhibited higher ultraviolet absorption, transparency, tensile strength, elongation at break, and water-resistance than the PS/PHF film. This indicated that the physical properties of the composites were greatly improved when the size of the fillers changed from microscale to nanoscale because the nanoscale size benefited their homogeneous dispersion in the matrix during the blending and film-forming process.

For the PHFNW-*t* nanowhiskers, the *L* and *D* decreased with an increase in *t*. The structure and properties of the PHFNW-*t* nanowhiskers and the corresponding PS/PHFNW-*t* films not only depend on the *L* and *D*, but also on the *L*/*D*. For example, the *L* and *D* of the PHFNW-8 (*t* = 8 h) is neither the shortest nor the longest among the prepared nanowhiskers; however, the corresponding PS/PHFNW-8 exhibited the highest transparency, tensile strength, and elongation at break among the PS/PHFNW-*t* films. This is due to PHFNW-8 having an *L*/*D* of 36.00, which is the highest among the PHFNW-*t*.

4. Conclusions

A series of pea hull fibre-derived nanowhiskers (PHFNW-*t*) was successfully extracted from pea hull fibres (PHF) by sulfuric acid hydrolysis with different hydrolysis times (*t*). The PHFNW-*t* was then blended with pea starch (PS) to prepare PS/PHFNW-*t* bionanocomposite films. With an increase in *t*, the length (*L*) and diameter (*D*) of the PHFNW-*t* decreased; while the *L*/*D* first increased, reaching the highest value when *t* = 8 h, and then decreased. Compared with the neat PS film and the PS/PHF (*t* = 0 h) film, the PS/PHFNW-*t* nanocomposite films showed higher ultraviolet absorption, transparency, tensile strength, elongation at break, and water-resistance. This is due to factors such as the nanometer size effects of the PHFNW-*t* (resulting from the nanoscale in *L* and *D*, the high *L*/*D*), the high content of cellulose crystalline regions, the homogeneous dispersion of PHFNW-*t* within PS, and the strong interaction between nanowhiskers and matrix. The PS/PHFNW-8 composite film exhibited the highest transparency, tensile strength and elongation at break among the series PS/PHFNW-*t* composite films. This is attributed to the PHFNW-8 having the highest *L*/*D* value among the PHFNW-*t*. In this work, it was found that 8 h was the most suitable time for hydrolysis of PHF with sulfuric acid in order to improve the elongation at break of the resulting bionanocomposite films.

Acknowledgements

This work was financially supported in part by Canadian Biomass Innovation Network (CBIN) TID 824, Agricultural Bioproducts Innovation Program of Canada via ABIP-140 to the Pulse Research Network (PURENet), and National Natural Science Foundation of China (NSFC 30570496). We also thank Jason Maley at the Saskatchewan Structural Sciences Centre (SSSC), University of Saskatchewan (Saskatoon, Canada) for providing the expertise for the AFM measurements.

References

Alemdar, A., & Sain, M. (2008). Isolation and characterization of nanofibers from agricultural residues – Wheat straw and soy hulls. *Bioresource Technology, 99*(6), 1664–1671.

Araki, J., Wada, M., Kuga, S., & Okano, T. (1998). Flow properties of microcrystalline cellulose suspension prepared by acid treatment of native cellulose. *Colloids and Surfaces A, 142*, 75–82.

Azizi Samir, M. A. S., Alloin, F., & Dufresne, A. (2005). Review of recent research into cellulosic whiskers their properties and their application in nanocomposite field. *Biomacromolecules, 6*(2), 612–626.

Beck-Candanedo, S., Roman, M., & Gray, D. G. (2005). Effect of reaction conditions on the properties and behavior of wood cellulose nanocrystal suspension. *Biomacromolecules, 6*, 1048–1054.

Bondeson, D., Mathew, A., & Oksman, K. (2006). Optimization of the isolation of nanocrystals from microcrystalline cellulose by acid hydrolysis. *Cellulose, 13*(2), 171–180.

Chazeau, L., Cavaillé, J. Y., Canova, G., Dendievel, R., & Boutherin, B. (1999). Viscoelastic properties of plasticized PVC reinforced with cellulose whiskers. *Journal of Applied Polymer Science, 1*(11), 1797–1808.

Chen, Y., Cao, X., Chang, P. R., & Huneault, M. A. (2008). Comparative study on the films of poly(vinyl alcohol)/pea starch nanocrystals and poly(vinyl alcohol)/native pea starch. *Carbohydrate Polymers, 73*, 8–17.

Chen, Y., Liu, C., Anderson, D. P., Huneault, M. A., & Chang, P. R. (2009). Pea starch-based composite films with pea hull fibres and pea hull fibre-derived nanowhiskers. *Polymer Engineering and Science*, in press, doi:10.1002/pen.21290.

Cheng, Q., Wang, S., Rials, T. G., & Lee, S. H. (2007). Physical and mechanical properties of polyvinyl alcohol and polypropylene composite materials reinforced with fibril aggregates isolated from regenerated cellulose fibres. *Cellulose, 14*(6), 593–602.

Choi, Y., & Simonsen, J. (2006). Cellulose nanocrystal-filled carboxymethyl cellulose nanocomposites. *Journal of Nanoscience and Nanotechnology, 6*(3), 633–639.

Dong, X. M., Kimura, T., Revol, J. F., & Gray, D. G. (1996). Effects of ionic strength on the isotropic-chiral nematic phase transition of suspensions of cellulose crystallites. *Langmuir, 12*(8), 2076–2082.

Dong, X. M., Revol, J. F., & Gray, D. G. (1998). Effect of microcrystallite preparation conditions on the formation of colloid crystals of cellulose. *Cellulose, 5*, 19–32.

Favier, V., Canova, G. R., Cavaillé, J. Y., Chanzy, H., Dufresne, A., & Gauthier, C. (1995). Nanocomposite materials from latex and cellulose whiskers. *Polymers for Advanced Technologies, 6*(5), 351–355.

Favier, V., Chanzy, H., & Cavaillé, J. Y. (1995). Polymer nanocomposites reinforced by cellulose whiskers. *Macromolecules, 28*(18), 6365–6367.

Frenot, A., Henriksson, M. W., & Walkenström, P. (2007). Electrospinning of cellulose-based nanofibres. *Journal of Applied Polymer Science, 103*(3), 1473–1482.

Gauthier, C., & Perez, J. (1995). Morphology and thermomechanical properties of latex films. *Polymers for Advanced Technologies, 6*(5), 276–284.

Hayashi, N., Kondo, T., & Ishihara, M. (2005). Enzymatically produced nano-ordered short elements containing cellulose Iβ crystalline domains. *Carbohydrate Polymers, 61*(2), 191–197.

Helbert, W., Cavaillé, J. Y., & Dufresne, A. (1996). Thermoplastic nanocomposites filled with wheat straw cellulose whiskers. Part I: Processing and mechanical behaviour. *Polymer Composites, 17*(4), 604–611.

Henriksson, M., Henriksson, G., Berglund, L. A., & Lindström, T. (2007). An environmentally friendly method for enzyme-assisted preparation of microfibrillated cellulose (MFC) nanofibres. *European Polymer Journal, 43*(8), 3434–3441.

Kvien, I., Tanem, B. S., & Oksman, K. (2005). Characterization of cellulose whiskers and their nanocomposites by atomic force and electron microscopy. *Biomacromolecules, 6*, 3160–3165.

Lu, Y., Weng, L., & Cao, X. (2006). Morphological, thermal and mechanical properties of ramie crystallites - Reinforced plasticized starch biocomposites. *Carbohydrate Polymers, 63*(2), 198–204.

Luo, L., Wang, X., Zhang, Y., Liu, Y., Chang, P., Wang, Y., et al. (2008). Physical properties and biocompatibility of cellulose/soy protein isolate membranes coagulated from acetic aqueous solution. *Journal of Biomaterial Science, Polymer Edition, 19*, 479–496.

Marchessault, R. H., Morehead, F. F., & Koch, M. J. (1961). Some hydrodynamic properties of neutral suspensions of cellulose crystallites as related to size and shape. *Journal of Colloid Science, 16*, 327–344.

Marchessault, R. H., Morehead, F. F., & Walter, N. M. (1959). Liquid crystal systems from fibrillar polysaccharides. *Nature, 184*, 632–633.

Mathew, A. P., & Dufresne, A. (2002). Morphological investigation of nanocomposites from sorbitol plasticized starch and tunicin whiskers. *Biomacromolecules, 3*(3), 609–617.

Nickerson, R. F., & Habrle, J. A. (1947). Cellulose intercrystalline structure. *Industrial & Engineering Chemistry, 39*, 1507–1512.

Pääkkö, M., Ankerfors, M., Kosonen, H., Nykänen, A., Ahola, S., Österberg, M., et al. (2007). Enzymatic hydrolysis combined with mechanical shearing and high-pressure homogenization for nanoscale cellulose fibrils and strong gels. *Biomacromolecules, 8*(6), 1934–1941.

Ranby, B. G. (1952). The cellulose micelles. *Tappi, 35*, 53–58.

Ratnayake, W. S., Hoover, R., & Warkentin, T. (2002). Pea starch: Composition, structure and properties – A review. *Starch/Stärch, 54*(6), 217–234.

Revol, J. F., Bradford, H., Giasson, J., Marchessault, R. H., & Gray, D. G. (1992). Helicoidal self-ordering of cellulose microfibrils in aqueous suspension. *International Journal of Biological Macromolecules, 14*, 170–172.

Roman, M., & Winter, W. T. (2004). Effect of sulfate groups from sulfuric acid hydrolysis on the thermal degradation behavior of bacterial cellulose. *Biomacromolecules, 5*(5), 1671–1677.

Sain, M., & Panthapulakkal, S. (2006). Bioprocess preparation of wheat straw fibers and their characterization. *Industrial Crops and Products, 23*(1), 1–8.

Sun, X. F., Xu, F., Sun, R. C., Fowler, P., & Baird, M. S. (2005). Characteristics of degraded cellulose obtained from steam-exploded wheat straw. *Carbohydrate Research, 340*, 97–106.

Takagi, H., & Asano, A. (2007). Characterization of "green" composites reinforced by cellulose nanofibres. *Key Engineering Materials, 334–335*(1), 389–392.

Tashiro, K., & Kobayashi, M. (1991). Theoretical evaluation of three-dimensional elastic constants of native and regenerated celluloses: Role of hydrogen bonds. *Polymer, 32*, 1516–1526.

Wang, B., Sain, M., & Oksman, K. (2007). Study of structural morphology of hemp fibre from the micro to the nanoscale. *Applied Composite Materials, 14*(2), 89–103.

Wang, N., Ding, E., & Cheng, R. (2007). Thermal degradation behaviors of spherical cellulose nanocrystals with sulfate groups. *Polymer, 48*(12), 3486–3493.

Ye, D. (2007). Preparation of nanocellulose. *Progress in Chemistry, 19*(10), 1568–1575.

Zhang, Y., & Han, J. H. (2006). Plasticization of pea starch films with monosaccharides and polyols. *Journal of Food Science, 71*, E253–E261.